Materials Transactions, Vol. 52, No. 3 (2011) pp. 554 to 559

EXPRESS REGULAR ARTICLE

Polycrystalline TiO_2 Thin Films with Different Thicknesses Deposited on Unheated Substrates Using RF Magnetron Sputtering

Ching-Hua Wei and Ching-Min Chang*

Department of Mechanical Engineering, Southern Taiwan University, Tainan 710, Taiwan, R. O. China

Different film thicknesses of polycrystalline TiO_2 thin films deposited on various unheated substrates using radio frequency (RF) magnetron sputtering is investigated. The crystalline structure, optical properties, and surface morphology and roughness were measured using an X-ray diffractometer (XRD), a field-emission scanning electron microscope (FESEM), an atomic force microscope (AFM), and a UV-Vis spectrophotometer. Polycrystalline phases were formed on unheated substrates due to the plasma particle bombardment. Crystalline structures more easily formed on the glass substrate and only nanocrystalline structures formed on the ITO glass substrate due to the surface roughness of substrates. The absorption edge and optical band gap depended on the crystalline particle size and phase structure. The XRD results indicate that 500-nm-thick film on a glass substrate had the strongest intensities of mixed anatase and rutile phases. [doi:10.2320/matertrans.M2010358]

(Received October 13, 2010; Accepted December 22, 2010; Published February 9, 2011)

Keywords: *titanium dioxide, film thickness, surface morphology, sputtering*

1. Introduction

Nano-structured semiconductor materials have attracted a lot of attention due to their unusual optical, electronic, and photoelectrochemical properties.[1–3] Nano-crystalline titanium dioxide (TiO_2) is one of the most investigated oxide materials due to its high refractive index, high dielectric constant, and optical transmittance in the visible and near-IR region.[4–6] It has been attracted a lot of interest for a wide range of applications, such as dye-sensitized solar cells,[7,8] photocatalysts,[5,9] optical coatings,[10,11] and capacitors for large-scale integrated (LSI) devices.[12] Fujishima and Honda discovered the photocatalytic decomposition of water on TiO_2.[5] Since then, the photocatalytic properties of TiO_2 have been studied intensively.[13–16] The hydrophilization on a TiO_2 thin film surface by UV light irradiation has also been investigated. When the photon energy exceeds the energy of the band gap, an electron (e^-) is promoted from the valence band to the conduction band, leaving a hole (h^+) behind. In semiconductors, some of these photoexcited electron-hole pairs diffuse to the surface and take part in chemical reactions with the adsorbed donor or acceptor molecules. The holes can oxidize donor molecules whereas the conduction band electrons can reduce acceptor molecules. Due to its wide band gap, TiO_2 has a strong oxidation power of generated holes, so they can react with water to produce highly reactive hydroxyl radicals ($^{\bullet}OH$). Both the holes and the ($^{\bullet}OH$) radicals are very efficient at oxidizing most organic contaminants.[17] Due to such superb properties, photocatalysts based on TiO_2 have been applied to the detoxification of water and air.[18,19]

TiO_2 is a wide bandgap oxide that occurs in three crystalline polymorphs: rutile (tetragonal), anatase (tetragonal), and brookite (orthorhombic).[20] Rutile is a tetragonal crystal with lattice parameters of $a = 0.4594\,nm$ and $c = 0.2958\,nm$, a refraction index of 2.7, and an optical band gap of 3.0 eV at room temperature. Anatase TiO_2 is a tetragonal crystal with lattice parameters of $a = 0.3785\,nm$ and $c = 0.9514\,nm$, a refraction index of 2.54, and an optical band gap of 3.2 eV at room temperature. Brookite is an orthorhombic crystal with lattice parameters of $a = 0.9184\,nm$, $b = 0.5447\,nm$, and $c = 0.5145\,nm$.[21] The photocatalytic activity of anatase is higher than that of rutile due to the former having a larger band gap (anatase $-3.2\,eV$, rutile $-3.0\,eV$).[22] TiO_2 films prepared by various methods, such as sol-gel processes,[23] the ion beam technique,[24] reactive sputtering,[25,26] electron beam evaporation,[27] chemical vapor deposition,[28] metal organic chemical vapor deposition (MOCVD),[29] plasma enhanced chemical vapor deposition (PECVD),[30] and radio frequency (RF) magnetron sputtering[31–33] have different crystalline structures that strongly depend on preparation conditions. Among thin film preparation methods, RF magnetron sputtering is one of the most easy to industrialize. It is suitable for optical coatings due to the high density, high adhesion, high hardness, and good thickness uniformity of the deposited layer over a large area. The structure and composition of TiO_2 thin films can be easily controlled by adjusting the deposition conditions. However, it is generally recognized that deposition on unheated substrates usually results in amorphous films.[31] Increasing the temperature to 473 K allows preparation of TiO_2 films with a crystalline structure.[34] The deposition of crystalline TiO_2 films on unheated substrates[32] could extend the range of film applications because it would allow the deposition of films directly onto a polymer or plastic surface. It is well known that high-power sputtered plasma produces secondary electrons that bombard thin films or substrates, causing them to heat up, which makes accurately controlling their temperature difficult. However, plasma particle bombardment induced the modification of film structure. It is meaningful to investigate the properties of TiO_2 thin films with different thicknesses deposited on unheated substrates.

In this paper, TiO_2 thin films were deposited onto unheated glass and indium tin oxide (ITO) glass substrates by RF magnetron sputtering. The crystalline phase, surface morphology and roughness, and optical properties of the

*Corresponding author, E-mail: d93z0204@webmail.stut.edu.tw

deposited films were observed using X-ray diffraction (XRD), field-emission scanning electron microscopy (FESEM), atomic force microscopy (AFM), and UV-Vis spectrophotometry, respectively. The effects of film thickness on the characteristics of TiO_2 thin films are discussed.

2. Experimental Procedure

2.1 Preparation of polycrystalline TiO_2 thin films

Polycrystalline TiO_2 thin films were prepared using an RF magnetron sputtering method with a TiO_2 ceramic target (High Purity Chemicals Lab. Corp., Grade: 99.99%, diameter: 100 mm, thickness: 5 mm) as the source material and Ar gas (99.995%) as the sputtering gas. An RF generator (PFG-300RF, Huttinger, Germany) operating at a frequency of 13.56 MHz and a power of 200 W was used. A stainless steel chamber was evacuated using a turbo pump to a base pressure less than 2.7×10^{-3} Pa. Ar gas was then introduced into the vacuum chamber as the working ambient by a mass flow controller (PC-540, Protec Instrument Inc.) at 40 sccm and kept at 1.1 Pa as the working pressure. Before the deposition of the samples, the chamber was kept in the pre-sputtering regime for 20 min (shutter closed) to remove contamination on the target surface in order to stabilize the deposition parameters. Samples denoted A_{gl}, B_{gl}, and C_{gl} were deposited onto a glass substrate, and samples denoted A_{ITO}, B_{ITO}, and C_{ITO} were deposited onto an ITO glass substrate. The area of sample was 20 mm × 20 mm. The sheet resistance of the ITO glass substrate was 7 Ω/□. Glass and ITO glass substrates were ultrasonically washed successively in acetone, isopropanol, alcohol, and deionized water each for 15 min. After the substrates were cleaned, they were statically placed on a sample holder facing the target at a fixed distance of 50 mm in a vacuum chamber. The sample holder with the substrates was neither heated nor rotated. The thickness of the thin films was monitored in real-time using a crystal thickness monitor (TM350, Maxtek, U.S.A.) during the deposition. Samples with film thicknesses of 100, 500, and 900 nm were prepared. In our experiment, the deposition rate was 3.2–5.4 nm/min and the deposition time was 30–160 min. The temperature of substrate due to the plasma particle bombardment was 423–430 K in the range of deposition time. Details of the deposition conditions of the polycrystalline TiO_2 thin films are summarized in Table 1.

2.2 Measurement and analysis methods

The film thickness d was determined using surface profilometry with a Surfcorder ET-4000M (Kosaka Laboratory Ltd., Japan) Alpha-step instrument. The crystal structures of the TiO_2 thin films were characterized by X-ray diffraction (XRD) using a Rigaku D/MAX 2500 diffractometer with Cu Kα ($\lambda = 0.15405$ nm) radiation under an applied voltage of 40 kV, a current of 100 mA, and an incident angle of 1° in the region of 20–80°. The grain sizes (D) listed in Table 1 were calculated from anatase (1 0 1) XRD reflections using the Debye-Scherrer equation:[35]

$$D = \frac{0.9\lambda}{B\cos\theta} \tag{1}$$

Table 1 Thickness, weight percentage of the anatase phase (W_A), grain size (D), surface roughness (R), and optical band gap (E_g) of the studied samples.

Sample	Thickness (nm)	W_A (%)	D (nm)	R (nm)	E_g (eV)
A_{gl}	100	—	—	1.11	3.27
A_{ITO}	100	—	—	2.48	3.38
B_{gl}	500	52	25	2.15	3.25
B_{ITO}	500	49	24	1.09	3.23
C_{gl}	900	40	34	1.68	3.26
C_{ITO}	900	100	36	1.78	3.25

where B is the peak width, θ is the diffraction angle, and λ is the X-ray wavelength corresponding to Cu Kα radiation. The fraction of the anatase phase, i.e., the weight fraction W_A of the anatase phase for samples consisting of both anatase and rutile phases, was calculated using the equation derived by Spurr and Mayers:[36]

$$W_A = \frac{1}{1 + 1.265(I_R/I_A)} \tag{2}$$

where I_A denotes the intensity of the strongest anatase reflection and I_R is the intensity of the strongest rutile reflection. For a given sample, the ratio I_A/I_R is independent of fluctuations in diffractometer characteristics.[36] In our experiments, the weight fraction (W_A) were calculated by eq. (2) and the results were summarized in Table 1. The surface morphological features of TiO_2 thin films were observed using a Hitachi S-4800 field-emission scanning electron microscope (FESEM). Before FESEM measurements, the sample surface was covered with a thin platinum film to prevent charge build-up. The surface roughness and surface morphology of the TiO_2 thin films were examined using atomic force microscopy (AFM) with an etched silicon cantilever in non-contact mode (Veeco, CP-II). The optical absorption spectra of the sputtered TiO_2 films were recorded using a UV-Vis spectrophotometer (Jasco Corporatin, Jasco V-670) in the wavelength range of 200 to 800 nm. Furthermore, optical band gaps of the films were calculated from the indirect allowed transition mode using the formula $\text{const}(h\nu - E_g)^2 = (4\pi\kappa/\lambda)h\nu$.[19]

3. Results and Discussion

3.1 X-ray diffraction measurements

Figure 1 shows the XRD patterns of TiO_2 films deposited on various unheated substrates. Each pair of samples, (A_{gl}, A_{ITO}), (B_{gl}, B_{ITO}), and (C_{gl}, C_{ITO}), was obtained from the same deposition run (same conditions) but on different substrates (glass and ITO glass, respectively). Figure 1(a) shows that the TiO_2 film is amorphous for sample A_{gl} and that sample B_{gl} has a mixed anatase and rutile structure. The grain size (D) and weight percentage (W_A) of the anatase phase are 25 nm and 52%, respectively, as calculated with eqs. (1) and (2). Sample C_{gl} also has a mixed anatase and rutile structure; the grain size (D) and weight percentage (W_A) are 34 nm and 40%, respectively. Generally speaking, crystalline structure of TiO_2 thin films needed to heat

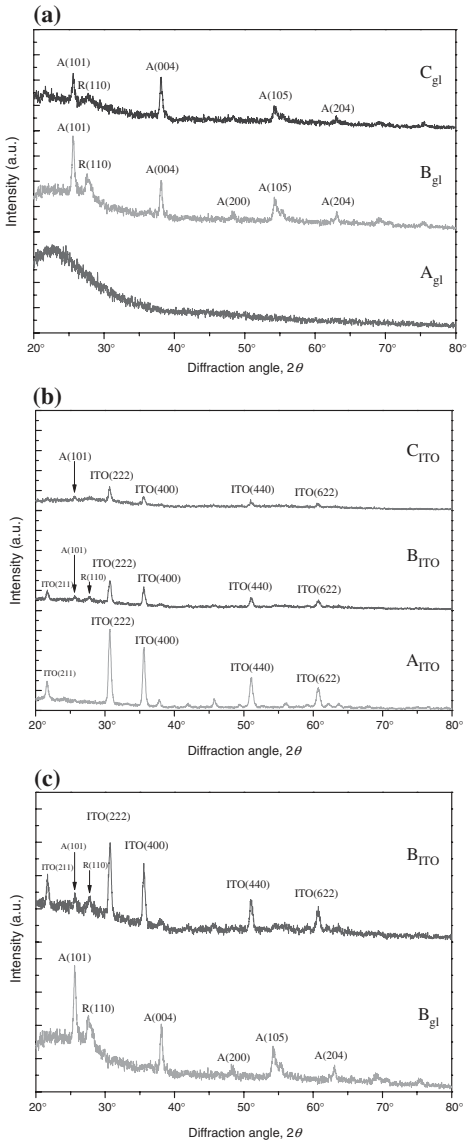

Fig. 1 XRD patterns of samples (a) A_{gl}-C_{gl}, (b) A_{ITO}-C_{ITO}, and (c) a comparison of B_{gl} and B_{ITO}.

substrates upto 473 K. In this study, crystalline structures of TiO_2 were successfully obtained by the temperature of plasma particle bombardment that was also found by Zeman *et al.*[37] The film changed from being amorphous to having a mixed structure with increasing film thickness. 500-nm-thick film thickness had a much stronger intensity of the mixed anatase and rutile structure than did 900-nm-thick film. Therefore, we suggest that the structure is related to film thickness on the glass substrate. Figure 1(b) shows that sample A_{ITO} has an amorphous TiO_2 film. Sample B_{ITO} has a mixed anatase and rutile structure, but the intensity is very small. Sample C_{ITO} has a weak-intensity anatase structure. The intensity of the characteristic peak of ITO glass decreased with increasing thickness of TiO_2 film. That is due to the thickness of the upper film affecting the lower film, as detected from the signal from the grazing incident angle method. The weak intensity of the mixed anatase and rutile structure indicates that the film grain size is on the nanoscale. Figure 1(c) shows a comparison of samples B_{ITO} and B_{gl}.

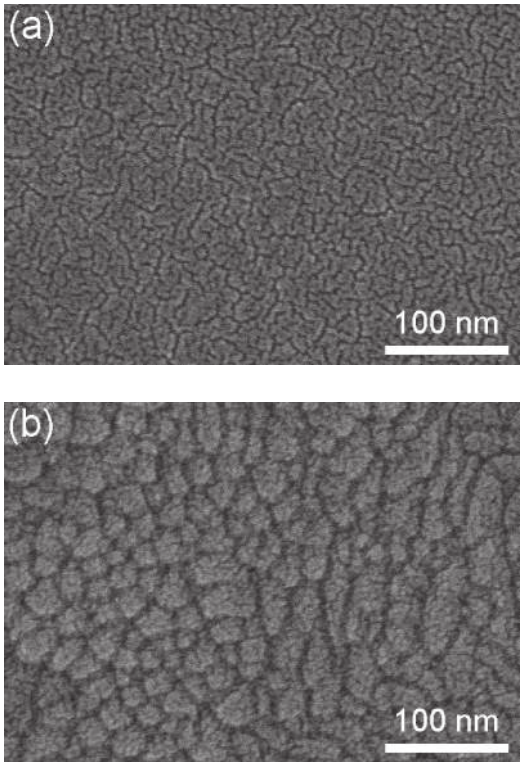

Fig. 2 Surface morphologies of glass (a) and ITO glass (b) substrates.

The crystallinity of films deposited under a given set of parameters depended on the type of substrate, which in consistent with results obtained in a previous study.[38]

3.2 SEM analysis

Figure 2(a) and (b) show the surface morphologies of glass and ITO glass substrates observed by FESEM, respectively. The glass substrate has a smooth surface, whereas the ITO glass substrate is rough due to its crystalline structure.

Figure 3(a)–(c) and (d)–(f) show FESEM images of TiO_2 thin films deposited at various thicknesses onto glass substrates (A_{gl}-C_{gl}) and ITO glass substrates (A_{ITO}-C_{ITO}), respectively. Sample A_{gl} was formed many cluster partly (Fig. 3(a)). Both sample B_{gl} (Fig. 3(b)) and sample C_{gl} (Fig. 3(c)) had a polycrystalline structure. However, the crystalline structure of sample B_{gl} was more polygonal than that of sample C_{gl}. Samples A_{ITO}-C_{ITO} (Fig. 3(d)–(f)) formed clusters over the entire surface of the thin film. The magnitudes of the average clustered size were calculated as 37.4 nm, 44.2 nm, and 43.8 nm, respectively. The results of Fig. 3(a)–(c) and 3(d)–(f) correspond to Fig. 1(a) and 1(b), respectively. The difference of surface morphology of TiO_2 thin films deposited onto glass and ITO glass substrates for a given set of parameters could be related to the growth mechanism of thin film for the sputter technique. It is well known that the film is deposited through nucleation, grain growth, coalescence, filling of channels, and film growth processes. The surface morphology of the ITO glass substrate had higher roughness and deeper crevices than those of the glass substrate. When TiO_2 particles were deposited on a substrate, they filled the crevices before the process of nucleation occurred. The crystalline phases formed more

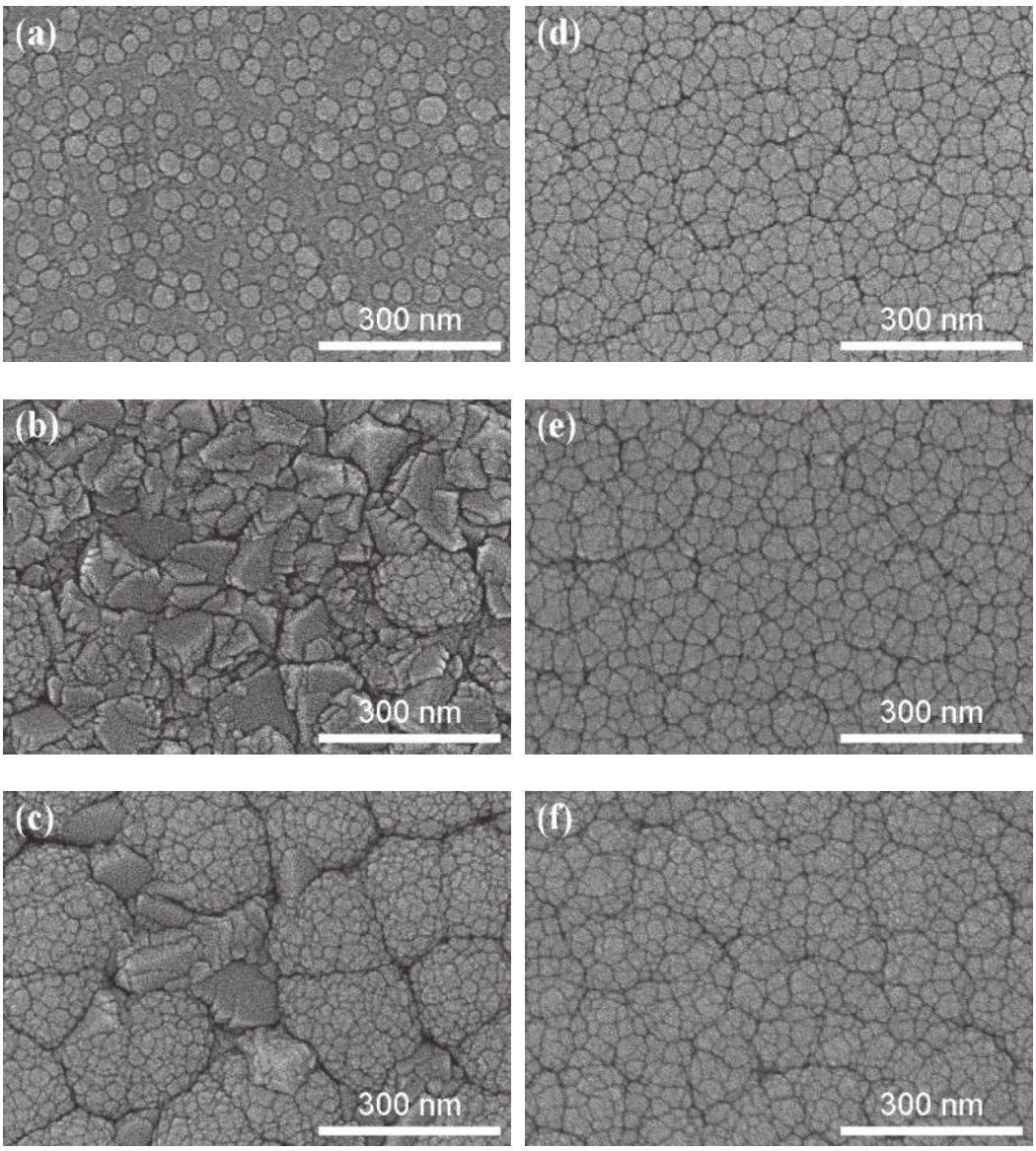

Fig. 3 FESEM images for (a)–(c) TiO_2 thin films deposited onto glass substrates (A_{gl}-C_{gl}) and (d)–(f) TiO_2 thin films deposited onto ITO glass substrates (A_{ITO}-C_{ITO}).

easily upon nucleation on the glass substrate than it did on ITO glass.

3.3 AFM analysis

The surface roughness of TiO_2 thin films deposited at various thicknesses onto glass substrates (A_{gl}-C_{gl}) and ITO glass substrates (A_{ITO}-C_{ITO}) was measured using AFM; the results are shown in Table 1. Theoretically speaking, the surface roughness of a crystalline structure is bumpier than that of an amorphous structure.[17] Therefore, sample B_{gl} had the bumpiest surface of the glass substrate samples; the value of roughness is 2.15 nm. The filling of crevices by TiO_2 particles deposited on ITO glass substrates could affect the surface roughness. Comparison Fig. 4(a) and (b), it shows the surfaces with a small cluster size (see Fig. 3(d)) were rougher than those with a large one (see Fig. 3(e)). Thus, sample A_{ITO} was the roughest of the ITO glass substrate samples; the value of roughness is 2.48 nm.

3.4 Optical properties

3.4.1 Absorption

Figure 5 shows the absorption spectrum of TiO_2 thin films deposited on glass (a) and ITO glass (b) substrates detected by a UV-Vis spectrophotometer with an integrating sphere in the wavelength range of 200 to 800 nm. Samples A_{gl}-C_{gl} and A_{ITO}-C_{ITO} both absorbed UV light (200–400 nm); the intensity of absorption increased with increasing film thickness. The discrepancy between absorption spectra in the range of 200–300 nm for samples A_{gl}-C_{gl} and A_{ITO}-C_{ITO} can be attributed to the difference of absorption between the glass substrate and ITO substrate. When the film thickness decreased, the absorption edges shifted to a shorter wavelength. Vorontsov[39] found that the absorption edge shifted to a shorter wavelength due to the quantum-size effect when the particle size was very small. Thus, we can deduce that the quantum-size effect influenced the absorption edges in our experiments.

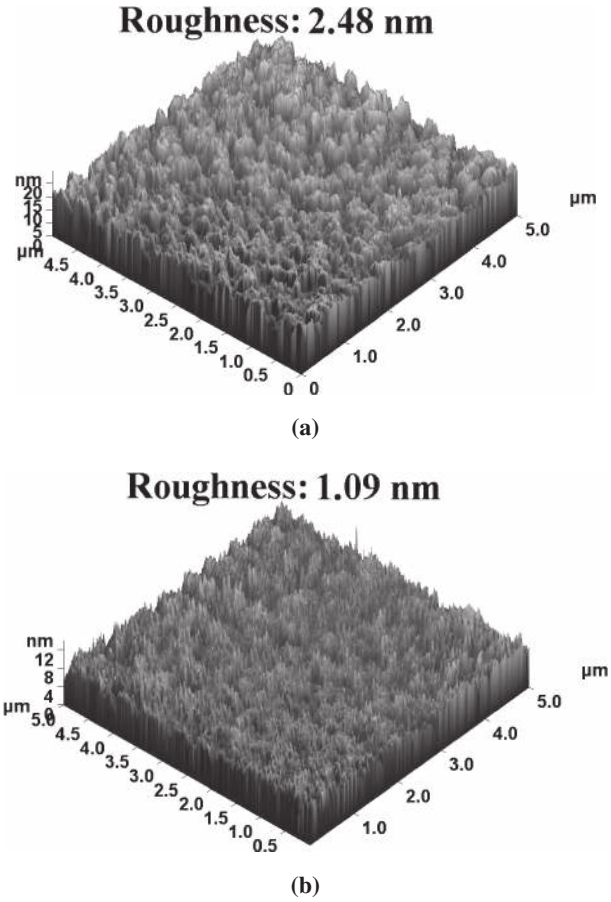

Fig. 4 AFM images for (a) and (b) TiO_2 thin films deposited onto ITO glass substrates (A_{ITO} and B_{ITO}).

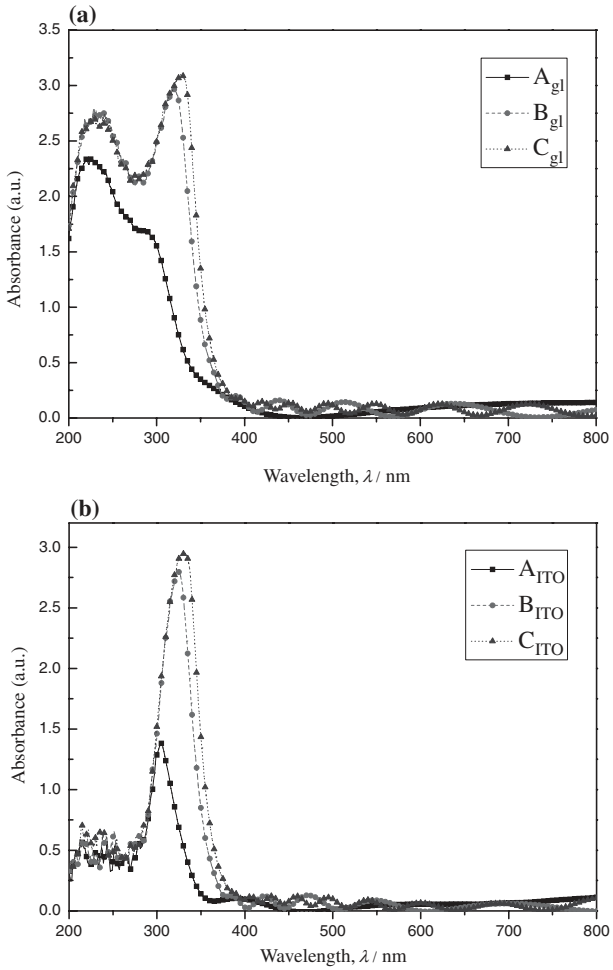

Fig. 5 Results of light absorption measurements for samples (a) A_{gl}-C_{gl} and (b) A_{ITO}-C_{ITO}.

3.4.2 Optical band gap

Close to the fundamental absorption, experimental results often satisfy the following relationship:[38]

$$\alpha = d^{-1} \ln(1/T) \tag{3}$$

where T is the transmittance, d is the thickness of the film, and α is the absorption coefficient at a photon energy $h\nu$.

The optical band gap, E_g, of TiO_2 films can be correlated to the absorption coefficient, α, using the Tauc expression for indirect allowed interband transitions:

$$const(h\nu - E_g)^2 = (4\pi\kappa/\lambda)h\nu \tag{4}$$

where $h\nu$ is the photon energy, $4\pi\kappa/\lambda$ is the absorption coefficient (α) at wavelength λ, and κ is the extinction coefficient. The Tauc plots of $(\alpha h\nu)^{1/2}$ as a function of the photon energy are shown in Fig. 6(a) and (b) for TiO_2 thin films deposited on glass and ITO glass substrates, respectively. The E_g value of the TiO_2 thin films can be obtained by extrapolating the linear portion of the curve to the photon energy axis, which is shown in Fig. 6. The optical band gap values are summarized in Table 1. The band gap of the 500-nm-thick film deposited on the glass substrate was the smallest (Fig. 6(a)), because the crystalline particle size influences the absorption edge of the thin film. For a small particle size, electrons in a nano-material exhibit different behavior from that in bulk materials. The properties of electrons in small particles depend on the crystallite size and shape due to the quantized motion of electrons and holes in a contained space.[40] As a result of the constraint, the band gap increases and the band edges shift.[41] The blue shift increases with decreasing particle size. Therefore, the quantum size effect influences the absorption edge. Our results are consistent with those reported in previous studies.[40,42] The band gap of the 500-nm-thick film deposited on the ITO substrate was the smallest (Fig. 6(b)), because of the mixed crystalline structure. According to reports by Diana *et al.*[38] and Pihosh *et al.*,[17] we can presume that the optical band gap of a mixed crystalline structure is smaller than that of a pure anatase structure.

4. Conclusion

The structure, optical properties, and surface morphology and roughness of polycrystalline TiO_2 thin films deposited at various thicknesses on unheated substrates by RF magnetron sputtering were investigated. The XRD results show that the crystalline structures vary with film thickness due to plasma particle bombardment. The intensity of mixed anatase and rutile structures was highest for the 500-nm-thick film deposited on a glass substrate. The SEM images and the roughness data obtained using AFM indicate that the surface morphology and roughness of glass and ITO glass substrates

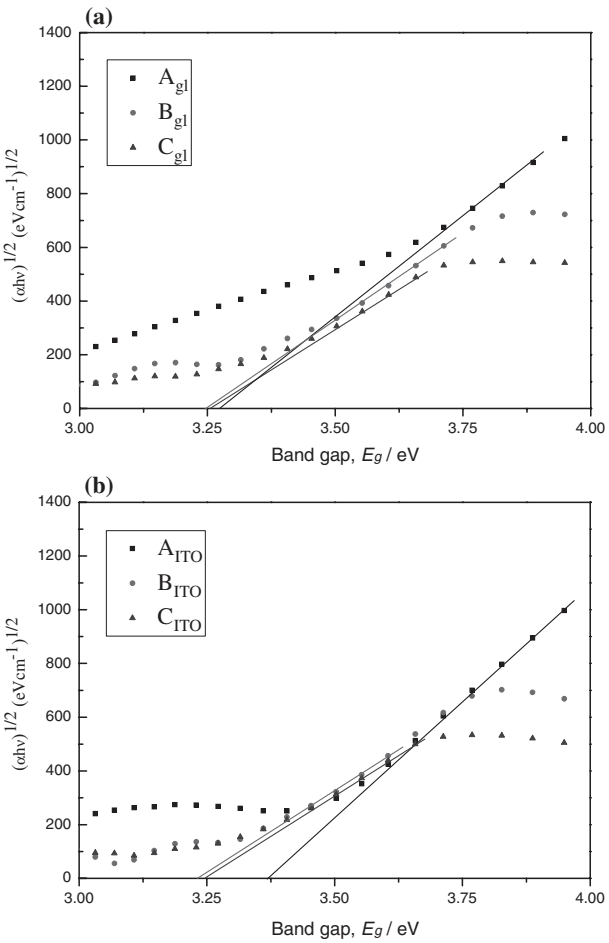

Fig. 6 Results of optical band gap measurements for samples (a) A_{gl}-C_{gl} and (b) A_{ITO}-C_{ITO}.

affect the properties of TiO_2 thin films. All prepared TiO_2 thin films absorbed UV light. The band gap of samples was calculated using the Tauc expression. The band gap of 500-nm-thick film deposited on glass and ITO glass substrates was the smallest. The thin films prepared in this study can be applied to flexible plastic substrates.

Acknowledgements

This work was supported by the National Science Council of the Republic of China under grant NSC 97-2622-E-218-005-CC3. We would like to thank the Optoelectronic Semiconductor Center and Nanotechnology Research Center at Southern Taiwan University for access to facilities. Valuable suggestions on this study from Dr. Wen-Tuan Wu, Dr. Wu-Chung Sue and Dr. Chin-Tu Lu were appreciated.

REFERENCES

1) L. J. Guo, X. Cheng and C. F. Chou: Nano Lett. **4** (2004) 69–73.
2) Q. Xu, B. D. Gates and G. M. Whitesides: J. Am. Chem. Soc. **126** (2004) 1332–1333.
3) P. Y. Liu, J. F. Chen and W. D. Sun: Vacuum **76** (2004) 7–11.
4) H. Kim, D. C. Gilmer, S. A. Campbell and D. L. Polla: Appl. Phys. Lett. **69** (1996) 3860–3862.
5) A. Fujishima and K. Honda: Nature **238** (1972) 37–38.
6) L. Forro, O. Chauvef, D. Emin, L. Zuppiroli, H. Berger and D. Levy: J. Appl. Phys. **75** (1994) 633–635.
7) B. O'Regan and M. Grätzel: Nature **353** (1991) 737–740.
8) A. Hagfelt and M. Gratzel: Chem. Rev. **95** (1995) 49–68.
9) A. Fujishima and K. Honda: Bull. Chem. Soc. Japan **44** (1971) 1148–1150.
10) K. Narashimha Rao and S. Mohan: J. Vac. Sci. Technol. A **8** (1990) 3260–3264.
11) K. Balasubramanian, X. F. Han and K. H. Guenther: Appl. Opt. **32** (1993) 5594–5600.
12) Y. H. Lee: Vacuum **51** (1998) 503–509.
13) C. D. Jaeger and A. J. Bard: J. Phys. Chem. **83** (1979) 3146–3152.
14) R. W. Matthews: J. Phys. Chem. **91** (1987) 3328–3333.
15) B. R. Weinberger and R. B. Garber: Appl. Phys. Lett. **66** (1995) 2409–2411.
16) H. Tada and M. Tanaka: Langmuir **13** (1997) 360–364.
17) Y. Pihosh, M. Goto, A. Kasahara and M. Tosa: Appl. Surf. Sci. **256** (2009) 937–942.
18) B. Weinberger and R. Garber: Appl. Phys. Lett. **66** (1995) 2409–2411.
19) N. Negishi, K. Takeuchi and T. Ibusuki: Appl. Surf. Sci. **121/122** (1997) 417–420.
20) H. Tang, K. Prasad, R. Sanjines, P. E. Schmid and F. Levy: J. Appl. Phys. **75** (1994) 2042–2047.
21) Y. Leprince-Wang and K. Yu-Zhang: Surf. Coat. Technol. **140** (2001) 155–160.
22) J. Augustynski: Electrochim. Acta **38** (1993) 43–46.
23) M. S. Park and M. Kang: Mater. Lett. **62** (2008) 183–187.
24) P. J. Martin: J. Mater. Sci. **21** (1986) 1–25.
25) E. Kusano and A. Kinbara: J. Appl. Phys. **87** (2000) 2015–2019.
26) E. Kusano and A. Kinbara: Thin Solid Films **281** (1996) 423–426.
27) C. Yang, H. Q. Fan, Y. X. Xi, J. Chen and Z. Li: Appl. Surf. Sci. **254** (2008) 2685–2689.
28) L. M. Williams and D. W. Hess: J. Vac. Sci. Technol. A **1** (1983) 1810–1819.
29) D. J. Won, C. H. Wang, H. K. Jang and D. J. Choi: Appl. Phys. A **73** (2001) 595–600.
30) M. Nakamura, K. Makino, L. Sirghi, T. Aoki and Y. Hatanaka: Surf. Coat. Technol. **169/170** (2003) 699–702.
31) L. Meng, M. Andritschky and M. Dos Santos: Thin Solid Films **223** (1993) 242–247.
32) I. Turkevych, Y. Pihosh, M. Goto, A. Kasahara, M. Tosa, S. Kato, K. Takehana, T. Takamasu, G. Kido and N. Koguchi: Thin Solid Films **516** (2007) 2387–2391.
33) K. Takamura, Y. Abe and K. Sasaki: Vacuum **74** (2004) 397–401.
34) L. Miao, P. Jin, K. Kaneko, A. Terai, N. Nabatova-Gabain and S. Tanemura: Appl. Surf. Sci. **212–213** (2003) 255–263.
35) L. Meng and M. Dos Santos: Thin Solid Films **226** (1993) 22–29.
36) R. Spurr and H. Myers: Anal. Chem. **29** (1957) 761–762.
37) P. Zeman and S. Takabayashi: Surf. Coat. Technol. **153** (2002) 93–99.
38) D. Mardare, M. Tasca, M. Delibas and G. I. Rusu: Appl. Surf. Sci. **156** (2000) 200–206.
39) A. V. Vorontsov, E. N. Savinov and J. Zhengsheng: J. Photochem. Photobiol. A: Chem. **125** (1993) 113–117.
40) T. M. Wang, S. K. Zheng, W. C. Hao and C. Wang: Surf. Coat. Technol. **155** (2002) 141–145.
41) M. R. Hoffmann, S. T. Martin, W. Choi and D. W. Bahnemann: Chem. Rev. **95** (1995) 69–96.
42) S. B. Amor, G. Baud, M. Jacquet and N. Pichon: Surf. Coat. Technol. **102** (1998) 63–72.